Izvestiya, Atmospheric and Oceanic Physics, Vol. 33, No. 1, 1997, pp. 16–26. Translated from Izvestiya AN. Fizika Atmosfery i Okeana, Vol. 33, No. 1, 1997, pp. 19–30.

Stability of an Axisymmetric Three-Layer Vortex

M. A. Sokolovskiy

Water Problems Institute, Russian Academy of Sciences, Novaya Basmannaya ul. 10, Moscow, 107078 Russia

Received March 31, 1995

Abstract—A stability of an isolated axisymmetric vortex is investigated within the framework of a three-layer quasi-geostrophic model on an *f*-plane. It is assumed that the potential vorticity of the layers is piecewise constant and is non-zero only inside initially circular areas (vortex patches) forming a three-layer vortex. The thickness of the layers, vortex patch radii, and density jumps at the upper and lower interfaces are arbitrary (the latter must only satisfy the steady stratification condition). The results of a linear analysis of vortex stability are tested using a three-layer modification of the contour dynamics method.

INTRODUCTION

The three-layer model of the ocean is the simplest approximation qualitatively describing the structure of a thermocline and an abyssal. In particular, the simplifications that are reasonable for the layered models make it possible to theoretically study the stability of currents and vortices with simple kinematic structures. The first publications devoted to investigation of the stability of a zonal three-layer flow bounded by vertical walls as applied to the atmosphere [1] and ocean [2] have initiated some generalizing works [3–5]. In particular, Smeed [5] has given a detailed review of earlier studies and analyzed the stability of a flow in a channel with arbitrary thicknesses h_1, h_2, and h_3 of the layers with constant densities ρ_1, ρ_2, and ρ_3 that satisfy the steady stratification condition (the layers are numbered downwards). The emphasis has been on the case $\Delta\rho_2/\Delta\rho_1 \ll 1$ ($\Delta\rho_n = \rho_{n+1} - \rho_n$, $n = 1, 2$), which is the most interesting case from the standpoint of applicability to the ocean. It has been shown that waves of two scales can exist: long waves connected with slopes of the upper interface and short waves generated by slopes of the lower interface. This conclusion has been confirmed in the accompanying experimental work [6], where results of laboratory research on the breaking of unstable three-layer vortices are presented. On the basis of a three-layer model with two active upper layers (at $h_1 = h_2$ and $h_1 \ll h_3$), Mirabel' and Monin [7, 8] have studied the stability of a large-scale ocean vortex and shown that triadic resonant interactions of breaking and explosive types are possible for waves of synoptic scales. Allowance for a continuous stratification [8, 9] has shown these results to be universal rather than induced by the three-layer approximation.

A problem of stability of an axisymmetric three-layer vortex with arbitrary h_n and ρ_n ($n = 1, 2, 3$) is considered below within the framework of the quasi-geostrophic model on an *f*-plane and under the rigid-lid condition at the surface. It is also assumed that the potential vorticity $\overline{\Pi}_n$, which is an adiabatic invariant, has an initially piecewise constant distribution of the form

$$\overline{\Pi}_n = \Pi_n \begin{cases} 1, & r \le \alpha_n \\ 0, & r > \alpha_n \end{cases}, \quad n = 1, 2, 3, \tag{1}$$

where Π_n are constants. The radii α_n of vortex patches in the layers are all different in the general case.

MAIN RELATIONS

We start from the statement of the problem of quasi-geostrophic three-layer vortex motions described in detail in [10]. For convenience, we present the main relations used below. Due to assumption (1), the pressure in the layers can be written as

$$p_n(x, y, t) = \Pi_n \oint_{C_n(t)} M(r) w d\nu_n + \sum_{j=2}^{3} q_{nj} \sum_{m=1}^{3} \Pi_m s_{jm} \oint_{C_m(t)} M_{j-1}(r) w d\nu_m, \quad n = 1, 2, 3. \tag{2}$$

Here, $r = ((x - x_1)^2 + (y - y_1)^2)^{1/2}$; x, y are the coordinates of the observation point; x_1, y_1 are the coordinates of the points of integration located on the contours C_n of initially circular vortex patches; $\nu_n(x_1, y_1)$ is a parameter continuously varying counterclockwise along the contour C_n; $M(r) = r^2(\ln r - 1/2)/4\pi$; $M_n(r) = (k_n r K_1(k_n r) - 1)/2k_n$, $n = 1, 2$; $w = ((x_1 - x)\dot{x}_1 - (y_1 - y)\dot{y}_1)/r_2$, where the point denotes partial differentiation with respect to ν_n; $K_n(\alpha)$ is the McDonald function of order n (hereinafter, without a special mention, we shall also use the modified Bessel functions $I_n(\alpha)$);

$$k_{1,2} = (-\lambda_{2,3})^{1/2} = [(G_1 \mp \sqrt{G_1^2 - 4G_2})/2]^{1/2};$$

$$G_1 = \frac{F_1}{h_1} + \frac{F_1 + F_2}{h_2} + \frac{F_2}{h_3}; \quad G_2 = \frac{F_1 F_2}{h_1 h_2 h_3};$$

$F_n = \rho_0(fL)^2(g\Delta\rho_n H)^{-1}$, L and H are the horizontal and vertical length scales; and the factors q_{ij}, s_{ij} $(i, j = 1,2,3)$ are the elements of the matrices Q and S, respectively, where $S = Q^{-1}$ and

$$Q = \begin{pmatrix} 1 & \dfrac{h_3\lambda_3}{\lambda_3 - \lambda_2} & -\dfrac{F_1}{h_1\lambda_3} \\ 1 & \dfrac{1}{\lambda_3 - \lambda_2}\left(h_3\lambda_3 + \dfrac{F_2}{h_2}\right) & -\left(\dfrac{F_1}{h_1\lambda_3} + 1\right) \\ 1 & \dfrac{1}{\lambda_3 - \lambda_2}\left(h_3\lambda_3 + \dfrac{F_2}{h_2} + \lambda_2 + \dfrac{F_1(h_1 + h_2)}{h_1h_2}\right) & -\left(\dfrac{F_1}{h_1\lambda_3} + 1 + \dfrac{h_2}{F_2}\left(\lambda_3 + \dfrac{F_1(h_1 + h_2)}{h_1h_2}\right)\right) \end{pmatrix}.$$

KINEMATIC STRUCTURE OF AN AXISYMMETRIC THREE-LAYER FLOW

It is clear that an arbitrary radial distribution of potential vorticity $\overline{\Pi}_n(r)$ in the layers determines a stationary state $p_n(r)$, $n = 1, 2, 3$. In the particular case (1), it is easy to obtain from (2) that the appropriate distributions of azimuth velocities have the form

$$V_n(r) = \sum_{j=1}^{3} q_{nj} \sum_{m=1}^{3} \Pi_m s_{jm} E_{j-1}^{(m)}(r), \quad n = 1, 2, 3, \quad (3)$$

where

$$E_0^{(m)} = \frac{1}{2}\begin{cases} r/\alpha_m, & r \le \alpha_m \\ \alpha_m/r, & r > \alpha_m, \end{cases}$$

$$E_l^{(m)} = \begin{cases} K_1(k_l\alpha_m)I_1(k_lr), & r \le \alpha_m \\ K_1(k_lr)I_1(k_l\alpha_m), & r > \alpha_m, \end{cases} \quad l = 1, 2.$$

Formula (3), as well as (2), manifests the interaction between all three vortex patches forming the three-layer vortex. In the framework of the model under consideration, this interaction occurs only due to the interface distortions described by the equations

$$\eta_n(x, y, t) = F_n(p_{n+1} - p_n), \quad n = 1, 2. \quad (4)$$

In the axisymmetric stationary case, it is obvious that $\eta_n = \eta_n(r)$.

A simple analysis shows that the interfaces η_1 and η_2 are horizontal planes only in the case of fulfillment of all the conditions: $\alpha_1 = \alpha_2 = \alpha_3$, $\Pi_1 = \Pi_2 = \Pi_3$, $\omega_1(r) = \omega_2(r) = \omega_3(r)$, where ω_i is the relative vorticity in the ith layer. Otherwise, distortions of these surfaces are inevitable. Having in mind a comparison with Smeed's results [5, 6], we shall obtain conditions when, for different Π_i, the local slopes of one of the interfaces are significantly greater than those of another interface.

We shall use the notions of *cone-shaped* and *cylinder-shaped* vortices, respectively, for the cases of different and equal radii α_1, α_2, α_3 of vortex patches. In the first case, six variants for the vertical structure of vortices are possible:

$$\begin{aligned} &1)\ \alpha_1 \ge \alpha_2 \ge \alpha_3, \quad 2)\ \alpha_1 \ge \alpha_3 \ge \alpha_2, \\ &3)\ \alpha_2 \ge \alpha_1 \ge \alpha_3, \quad 4)\ \alpha_2 \ge \alpha_3 \ge \alpha_1, \\ &5)\ \alpha_3 \ge \alpha_1 \ge \alpha_2, \quad 6)\ \alpha_3 \ge \alpha_2 \ge \alpha_1. \end{aligned} \quad (5)$$

The second case of a cylinder-shaped vortex $\alpha_1 = \alpha_2 = \alpha_3$ is apparently common for all variants (5). In this paper, the emphasis is on this specific case in view of the analogy with the problem of a flow in a channel whose stability was examined in the majority of the studies cited in the Introduction.

It is easy to obtain conditions when the following inequalities are valid for a vortex with $\alpha_1 = \alpha_2 = \alpha_3$

$$\left|\frac{\partial\eta_1}{\partial r}\right| \gg \left|\frac{\partial\eta_2}{\partial r}\right| \ \text{ or } \ \left|\frac{\partial\eta_2}{\partial r}\right| \gg \left|\frac{\partial\eta_1}{\partial r}\right|. \quad (6)$$

Actually, it is seen from (3) that, since all functions $E_j(r)$, $j = 0, 1, 2$, determining the radial structures of velocities are equal to zero at $r = 0$, tend to zero as $r \longrightarrow \infty$, and have a maximum at $r = 1$, situations (6) should be expected when

$$V_2(1) = V_3(1) \ \text{ or } \ V_1(1) = V_2(1), \quad (7)$$

respectively.

Equations (3) indicate that, at any r = const, the azimuth velocities depend linearly on the potential vorticities Π_m or on W_m, $m = 1, 2, 3$, which is equivalent. The meaning of the variables W_m is clear from the relation for vortex integral intensity C

$$C = \sum_{m=1}^{3} \alpha_m^2 h_m \Pi_m \equiv W_1 + W_2 + W_3. \quad (8)$$

Some plots in this and the following section are drawn in the (W_1, W_3)-plane at $W_2 = 1$. For example, Fig. 1 shows a set of straight lines along which the above relations between $V_m(1)$ for different $m = 1, 2, 3$

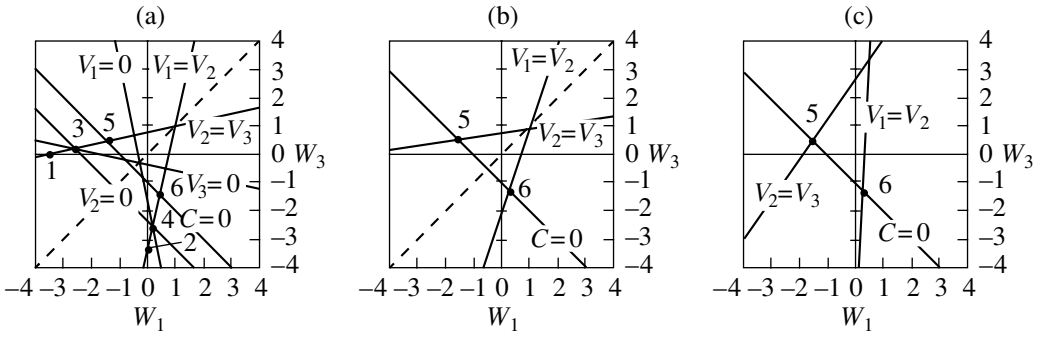

Fig. 1. Straight lines that are described by the relations indicated in them between the azimuth velocities in the contours of circular vortex patches in the layers at $h_1 = h_2 = h_3 = 1/3$; (a) $F_1 = F_2 = 1$; (b) $F_1 = 1$, $F_2 = 4$; and for (c) $h_1 = 0.1$, $h_2 = 2$, $h_3 = 0.7$; $F_1 = 1$, $F_2 = 4$. The numbering of the points is explained in the text.

occur. For brevity, relations of the type of $V_1(1) = 0$, $V_1(1) = V_2(1)$, etc. are written down as $V_1 = 0$, $V_1 = V_2$, respectively. Here, the straight line is represented at all points of which the quantity C from (8) vanishes. The numbered intersection points correspond to the simultaneous fulfillment of the conditions indicated in artificial breaks of the appropriate lines. For example, the first of conditions (7) can be supplemented by the requirements $W_3 = 0$ (point 1), $V_2(1) = V_3(1) = 0$ (point 3), and $C = 0$ (point 5). The points with even numbers belong to the straight line $V_1(1) = V_2(1)$ —the second of conditions (7). The following plot that is drawn for the external parameters corresponding to points 5 (Fig. 2a) and 6 (Fig. 2b) demonstrates the validity of the statement about the accordance of conditions (6) and (7). Figure 3 gives a good idea about the structure of the radial profile of azimuth velocities in the layers; here examples of dependence (3) for the cylinder-shaped (Figs. 3a–3e) and cone-shaped (Figs. 3f–3h) vortices are presented. It is seen that the interaction between the vortex patches results in an essential modification of the fields of the relative vorticity, whose sign can frequently be opposite to the sign of the corresponding potential vorticity.

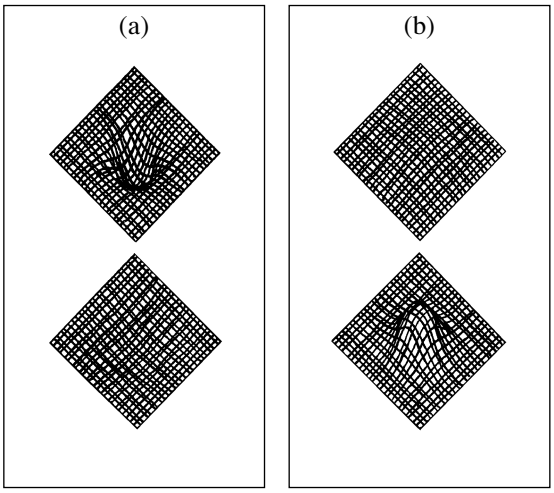

Fig. 2. Isometric projection of the interfaces between the layers η_1 (top) and η_2 (bottom) for (a) the first and (b) second conditions (7), when the external parameters correspond to points 5 and 6 in Fig. 1a, respectively.

It is shown below that all vortices of the structure presented in Fig. 3 are unstable, which results in their breakup during their evolution.

LINEAR STABILITY ANALYSIS

We describe the general scheme of stability analysis for an axisymmetric three-layer vortex with relatively small azimuth perturbations in the shape of the vortex patches forming the vortex. Let the lines of constant potential vorticities in polar coordinates (r, θ) have a parametric representation of the type

$$r = f_n(\theta, t; \alpha_n), \quad n = 1, 2, 3, \tag{9}$$

with $\alpha_n = f_n(\theta, 0; \alpha_n)$. The total differentiation of (9) with respect to time gives the equations

$$f_n f_{n,t} + V_n^{(\theta)} f_{n,\theta} - V_n^{(r)} f_n = 0, \quad n = 1, 2, 3, \tag{10}$$

where $V_n^{(\theta)}$ and $V_n^{(r)}$ are the azimuth and radial components of velocities in the nth layer, and the subscripts t and θ denote partial differentiation with respect to the appropriate variables.

Assuming that

$$\begin{aligned} f_n(\theta, t; \alpha_n) &= \alpha_n + \varepsilon_n(\theta, t; \alpha_n), \quad |\varepsilon_n| \ll 1, \\ \varepsilon_n(\theta, t; \alpha_n) &= A_n(\alpha_n)\exp(i(\gamma_m t + m\theta)), \quad m \geq 1, \end{aligned} \tag{11}$$

we linearize equation (10) and obtain a set of dispersion relations

$$\gamma_m + \frac{m}{\alpha_n}\sum_{j=1}^{3} q_{nj}(P_{j-1}(\alpha_n)A_n(\alpha_n) + iR_{j-1}^{(m)}(\alpha_n)) = 0, \quad n = 1, 2, 3, \quad m \geq 1, \tag{12}$$

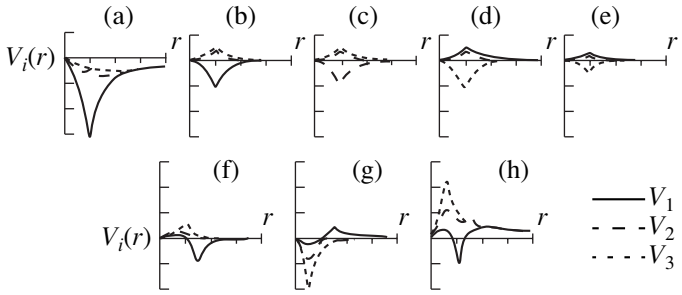

Fig. 3. Radial structures of azimuth velocities (3) for cylinder-shaped vortices under the conditions corresponding to the points in Fig. 1a: (a) 1, (b) 5, (c) 6; to the points in Fig. 1b: (d) 5, (e) 6, and for cone-shaped vortices at (f) $h_1 = 0.1$, $h_2 = 0.2$, $h_3 = 0.7$: $W_1 = -2$, $W_3 = 0$, $\alpha_1 = 1.5$, $\alpha_2 = 1$, $\alpha_3 = 0.5$; (g) $W_1 = 1$, $W_3 = -1$, $\alpha_2 = 1.5$, $\alpha_2 = 1.5$, $\alpha_3 = 0.5$; and (h) $W_1 = -1$, $W_3 = 1$, $\alpha_2 = 1$, $\alpha_2 = 1.5$, $\alpha_3 = 0.5$.

where

$$P_{j-1} = \sum_{k=1}^{3} s_{jk} \int_0^\infty \overline{\Pi}_k(\beta)\beta \frac{\partial J_{j-1}^{(0)}}{\partial r}(r, \beta)d\beta,$$

$$R_{j-1}^{(m)} = \frac{m}{r}\sum_{k=1}^{3} s_{jk} \int_0^\infty \overline{\Pi}_k'(\beta)A_k(\beta)\beta J_{j-1}^{(m)}(r, \beta)d\beta,$$

$$J_j^{(l)} = \begin{cases} \ln\beta \\ \ln r \end{cases}; -\frac{1}{2l}\begin{cases} (r/\beta)^l \\ (\beta/r)^l \end{cases}; -\left.\begin{cases} I_l(k_j r)K_l(k_j\beta) \\ I_l(k_j\beta)K_l(k_j r) \end{cases}\right| \begin{matrix} r \le \beta \\ r > \beta, \end{matrix} \quad (13)$$

$$l = 0, \qquad l \ge 1, \qquad l \le 0,$$
$$j = 0, \qquad j = 0, \qquad j = 1, 2.$$

The condition for the solvability of set (12) gives the characteristic equation

$$|B - \gamma_m E| = 0, \quad (14)$$

where E is the identity matrix, and B is the third-order matrix whose elements, under assumption (1), have the form

$$b_{nj} = \sum_{k=1}^{3} s_{kn}\left(q_{nk}T_{kn}^{(k-1)}\Pi_j - \delta_{nj}\frac{m}{\alpha_n}U_{k-1}(\alpha_n)\right), \quad (15)$$

$$n, j = 1, 2, 3.$$

Here δ_{nj} is Kronecker's delta, $T_{nn}^{(0)} = 1/2$, and $T_{nn}^{(1,2)} = mI_m(k_{1,2}\alpha_n)K_m(k_{1,2}\alpha_n)$, $(n = 1, 2, 3)$. The quantities U_j and the other $T_{in}^{(j)}$ depend on the shape of the vortex under study and are calculated in each specific case as the appropriate combinations of integrals of functions similar to (13) with the locking properties of Heaviside's function and the puncturing properties of delta function taken into account. These relations for the first of variants (5) are listed in the Appendix as an example.

It is seen from (11) that the instability condition for a mode with number m is determined by the inequality $\mathrm{Im}\,\gamma_m < 0$, which appears to occur only if a single real root of the cubic equation for γ_m resulting from (14) exists. Its solutions and, consequently, the stability properties of the vortex depend on 11 external parameters: α_n, Π_n, h_n $(n = 1, 2, 3)$, F_1, F_2. The number of these parameters can be reduced, because only the relative horizontal sizes of the vortex patches and the relative potential vorticities are important for the analysis. We have already fixed the Π_2 value setting $W_2 = 1$. We also assume that the radius of a mean-size vortex patch in the nth layer is equal to unity, i.e., $\alpha_{\min} \le \alpha_n = 1 \le \alpha_{\max}$. Finally, we note that only two of the h_n values can be chosen independently, whereas the third is determined from the relation $h_1 + h_2 + h_3 = 1$. Thus, the number of independent external parameters can be reduced to eight.

RESULTS OF A STABILITY ANALYSIS

Solution (14) allows us to single out instability domains bounded by neutral hypersurfaces in the space of external parameters. Their sections by the (W_1, W_3)-plane with other parameters specified are presented in the right parts of Figs. 4 and 3. The curves of neutral stability are plotted by bold lines; internal parts of the boundaries of the instability domains are shaded by points. The numbered points of Fig. 1 whose azimuth-velocity profiles are plotted in Figs. 3a–3e are transferred into Fig. 4. The points corresponding to the azimuth-velocity profiles presented in Figs. 3f, 3g, and 3h are labeled in Fig. 5 by Roman figures I, II, and III, respectively. The schematic images of vertical sections of the vortices are drawn in the left parts of both figures. It is evident that they have little in common with the vortex structure (especially for the cone-shaped vortex) and only characterize the relationship between an unperturbed thickness of layers, the radii of vortex patches, and (conventionally) the densities of the layers—the extent of stratification is displayed by intensity of shading.

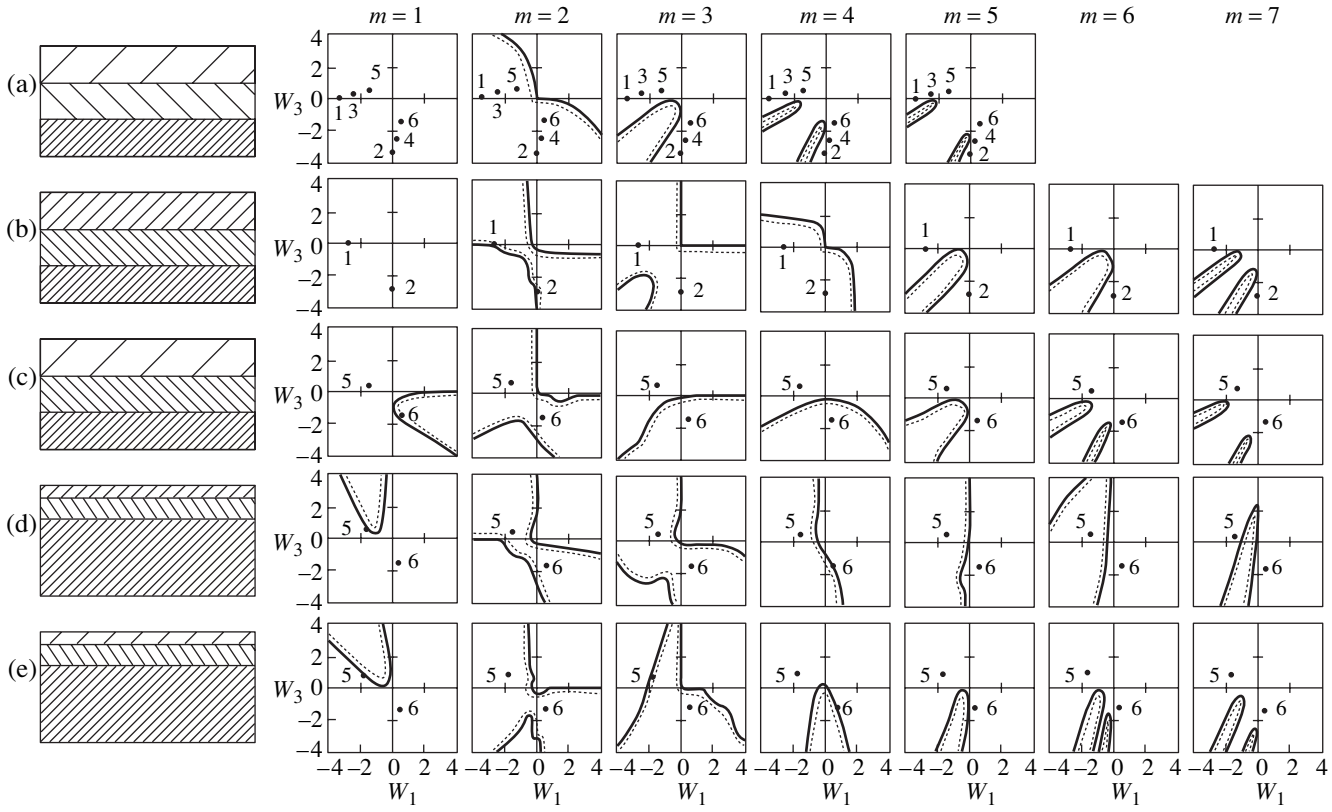

Fig. 4. Schematic vertical sections (left) and projections onto the (W_1, W_3)-plane of the curves of neutral stability for the cylinder-shaped vortices for several first azimuth modes (right) at $W_2 = 1$ and $h_1 = h_2 = h_3 = 1/3$: (a) $F_1 = F_2 = 1$, (b) $F_1 = F_2 = 4$, (c) $F_1 = 1$, $F_2 = 4$; and for $h_1 = 0.1$, $h_2 = 0.2$, $h_3 = 0.7$: (d) $F_1 = F_2 = 4$, (e) $F_1 = 1$, $F_2 = 4$.

Cylinder-Shaped Vortex

An analysis shows that, at $F_1 = F_2 \equiv F$ (i.e., at $\Delta\rho_1 = \Delta\rho_2 \equiv \rho$) and for layers of an equal unperturbed thickness, only modes with $m \geq 2$ can be unstable, and an increase in F (decrease in $\Delta\rho$) contributes to the instability of the higher modes of perturbations. In particular, this is seen from a comparison of Figs. 4a and 4b. The modes with

$$m \propto F^{1/2}, \tag{16}$$

are found to be the most unstable. Actually, it is easy to see that, if $F_1 = F_2$, the elements of the matrices Q and S do not depend on F; therefore, the effects of stratification in (15) are described only by the terms $T_{nn}^{(1,2)}$, which take the form $mI_m(k_{1,2})K_m(k_{1,2})$ in this case. Due to their asymptotic properties, these functions give a finite contribution only for $m \propto k_{1,2}$, whence relation (16) follows. Thus as $F \longrightarrow \infty$, only perturbations with infinitesimally small wavelength can be unstable. Similar to [3], the stabilization is observed for small F (profound stratification), and all the modes become steady as $F \longrightarrow 0$. These two limiting cases prove to be close (in the sense indicated), which can be explained by the fact that pressures (2) in each layer are determined by the barotropic logarithmic Green's function both as $F \longrightarrow \infty$ and as $F \longrightarrow 0$. The first case corresponds to the model of a homogeneous ocean, whereas the second case corresponds to the model of a three-layer ocean with infinite jumps in density $\Delta\rho$. As applied to the two-layer quasi-geostrophic model, this was first noted in [11].

If $F_1 \neq F_2$ (Fig. 4c), the instability of the $m = 1$ mode is possible. However, an analysis of growth rates $|\gamma_m|$ of various modes shows that, apparently, the instability conditions of the first mode can not be realized. A fundamental difference of this case from those considered above is the asymmetry of instability domains about the straight line $W_1 = W_3$. This shows different roles of distortions of the upper and lower interfaces in the formation of the scale of perturbations generated due to the instability. Actually, point 5, for example, where $|\partial n_1/\partial r| \gg |\partial n_2/\partial r|$, now belongs only to the instability domain of the $m = 2$ mode, while in point 6, where an opposite condition is fulfilled, the modes with $m = 1, 2, 3, 4$ are unstable.

The situation with layers of different thickness is more realistic. Assuming that the main thermocline is modeled by two upper layers, we set $h_1 = 0.1$, $h_2 = 0.2$, and $h_3 = 0.7$. For a mean ocean depth of 4 km, this gives the depth of the lower boundary of the thermocline

equal to ∝1.3 km, which is quite typical for the ocean [12]. According to Fig. 4d, even at $F_1 = F_2$, there is a theoretical possibility for the $m = 1$ mode to be unstable. In addition, the mutual arrangement of points 5 and 6 and the estimation of the corresponding growth rates $|\gamma_m|$ lead to the conclusion that the fifth and the third modes are the most unstable in the first and in the second cases, respectively (an effect that is opposite to that described above). However, we note that the assumption that the density jumps are equal is too unnatural for such a relationship between layers' thicknesses. If $F_1 < F_2$ (Fig. 4e), again prevailing slopes of the lower interface contribute to the generation of more short-wavelength perturbations, which confirms the above-cited Smeed's conclusion [5, 6]. Here, similar maxima of the growth rates of unstable perturbations at points 5 and 6 are reached for $m = 2$ and $m = 3$ modes, respectively.

Cone-Shaped Vortex

The stability of vortices of type of (5) is studied in the simplest case when $|\alpha_1 - \alpha_2| = |\alpha_2 - \alpha_3| = \Delta\alpha$. Selected results are presented in Fig. 5.

A comparison of Figs. 4a, 5a, and 5b, where $F_1 = F_2 = 1$, $h_n = 1/3$, $n = 1, 2, 3$ and only $\Delta\alpha$ values are different, allows us to conclude that, as the three-layer vortex structure becomes increasingly different from a cylinder-shaped vortex, the instability domains are displaced towards the lowest modes. If $\Delta\alpha \neq 0$, the instability of the $m = 1$ mode becomes, as a rule, dominant even in the domains of intersection. The instability of the first twisting mode [13] must manifest itself as a result of a horizontal relative shift of vortex patches (i.e., of the slope of the eddy axis) and of a subsequent rotation of the eddy as a whole around its fixed center of gravity.

Turning to a weaker stratification (Fig. 5c), to the case of $F_1 < F_2$ (Fig. 5d), and to a more realistic relationship between layer thicknesses (Figs. 5d–5g), does not lead to considerable qualitative changes in the stability properties of the vortex. It is seen that, among the points singled out, point II alone is characterized by the only unstable mode with $m = 1$. According to an analysis of the growth rates of unstable perturbations, of two first modes, the second one is dominant for point I, and the first one is dominant for point III.

SIMULATION OF UNSTABLE VORTEX EVOLUTION

The break of unstable vortices was studied with the method of contour dynamics extended to the case of a three-layer fluid [10].

In computations, a set of marker points N_n was specified in each contour C_n from (2). The equations of motion for Lagrangian particles that are coincident with these points take the form

$$\frac{d}{dt}r_l^{(n)} = V_l^{(n)}, \quad l = 1, 2, \ldots, N_n, \quad n = 1, 2, 3. \quad (17)$$

The expressions for the right-hand sides of (17) can be obtained from (2) by using the geostrophic relations. The initial conditions were determined by specifying the radius-vectors of the marker points distributed uniformly along the initially circular contours C_n. The number of the marker points was chosen such that 52 nodes were in the circle of unit radius. In all the computations, the initial distributions of the potential vorticities in the layers corresponded to the situations marked by the numbered points in Figs. 4 and 5. "Computer noise" that necessarily accompanies any computation due to the errors of numerical interpolation, differentiation, integration of discrete functions, etc., was the only source of perturbations.

The ordinary differential equations (17) were solved by the Runge–Kutta method of the fourth order of accuracy with step $\Delta t = 0.1$ using "optimum" Gill's formulas [14]. Makarov's program codes [15] and the contour "surgery" technique developed by him [16] were used as the basic elements of the method of contour dynamics computations. The latter technique allows us to cut off long and thin vortex filaments and also to remove extra parts of boundaries when vortices of equal potential vorticities merge. This technique allows for a mechanism of artificial dissipation and ignores the vortices whose contours contain a number of nodes smaller than a preassigned number $N_m = N_{\min}$ (we assumed that $N_{\min} = 6$).

The results of computations are presented in the figures as synchronous configurations of contours of the top, middle, and bottom layers plotted sequentially from top to bottom within separate frames for the indicated instants of dimensionless time.

Cylinder-Shaped Vortex

Figures 6a and 6b show two examples of the break of three-layer vortices in the case when the second mode is only unstable and also the first of conditions (6) is fulfilled at the initial instant. When the bottom layer is dynamically passive (Fig. 6a), we observe the formation of a structure that resembles a tripole in a barotropic fluid [17]. The distinction is that, in the case under consideration, the central anticyclonic vortex is located in the top layer, and its two satellites—cyclones—are located in the middle layer. These satellites periodically approach each other and move away rotating counterclockwise together with a pulsating quasi-elliptic vortex that is located above and keeps its simply-connected structure. The contours of the bottom layer play the role of marker lines deformed due to the velocity field induced by top eddies. The shape of the resulting vortex structure resembles a *carousel* containing seats

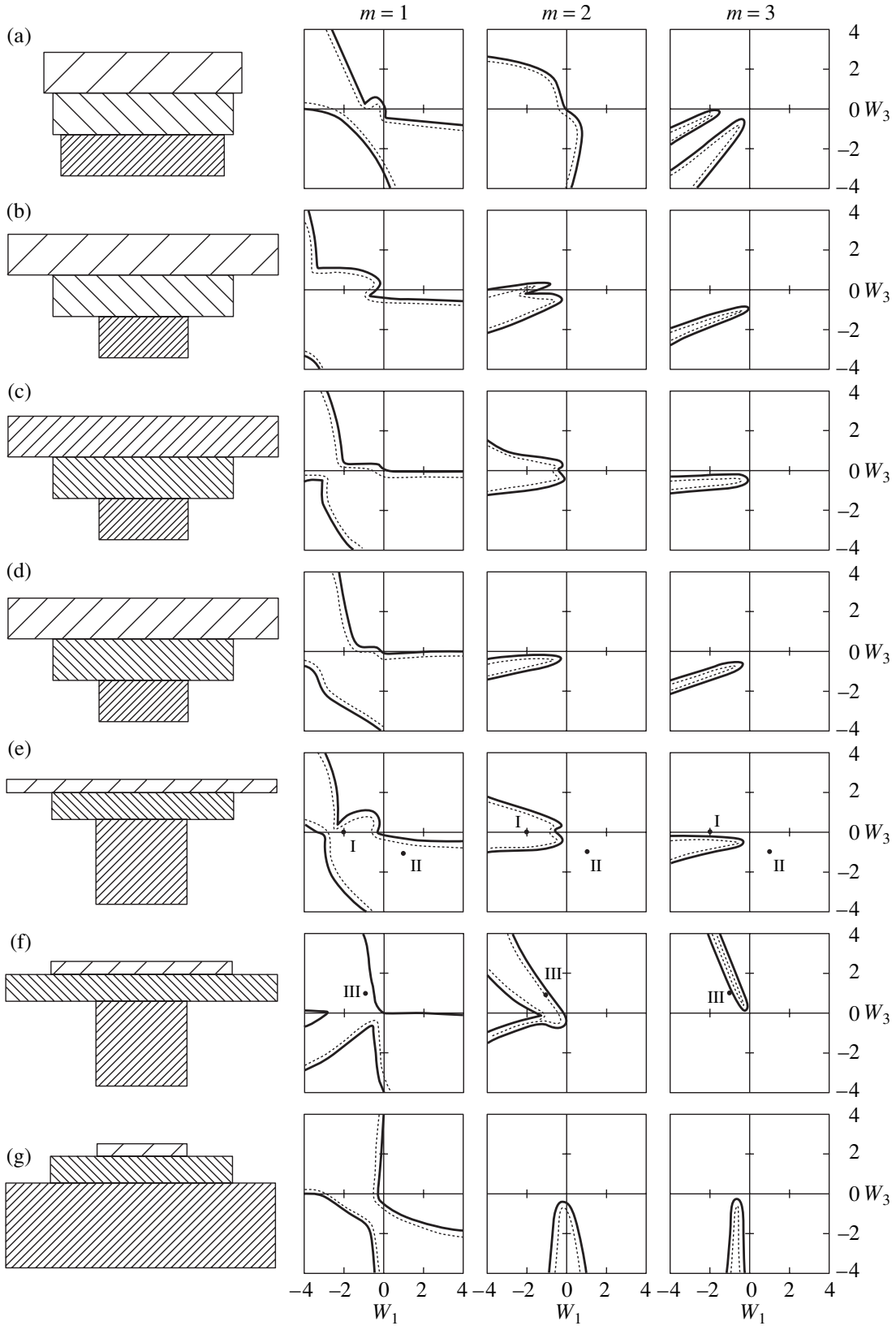

Fig. 5. The same as in Fig. 4 but for cone-shaped vortices at $h_1 = h_2 = h_3 = 1/3$, $\alpha_1 > \alpha_2 > \alpha_3$: (a) $\Delta\alpha = 0.1$, $F_1 = F_2 = 1$, (b) $\Delta\alpha = 0.5$, $F_1 = F_2 = 1$, (c) $\Delta\alpha = 0.5$, $F_1 = F_2 = 4$, (d) $\Delta\alpha = 0.5$, $F_1 = 1$, $F_2 = 4$, and at $h_1 = 0.1$, $h_2 = 0.2$, $h_3 = 0.7$, $\Delta\alpha = 0.5$, $F_1 = 1$, $F_2 = 4$: (e) $\alpha_1 > \alpha_2 > \alpha_3$, (f) $\alpha_2 > \alpha_1 > \alpha_3$, (g) $\alpha_3 > \alpha_2 > \alpha_1$.

suspended by swivels from a disk rotating around the vertical axis. The seats are, in turn, capable of rotating around their instantaneous axes. Thus, we observe a stratified analogue of the tripole much as alignment [18] is a two-layer analogue of vortex merging.

The next numerical experiment differs from the previous one in that the condition $W_3 = 0$ is replaced by $C = 0$. In this case (Fig. 6b), after the break of vortex patches in the layers (in the series of images displayed, the vortex patch in the bottom layer has not yet broken down), the rotation around the common center of gravity stops, and a vortex patch is formed composed of two three-layer vortices with bow-shaped axes (we use the terminology by Gryanik and Tevs [19]). These vortices move in opposite directions along a fixed straight line.

We note that the dissimilarity of these two scenarios of unstable vortex break is caused only by the difference in the appropriate distributions of the potential vorticity along the vertical. This confirms the conclusion of Verron, McWilliams, and Hopfinger [20] about an important role of initialization of vortices.

In the symmetric case (by terminology from [19]) $h_1 = h_2 = h_3$ and $F_1 = F_2$, the interfaces η_1 and η_2 play the same role. This is shown in Fig. 6c, where the initial state is now given by the second condition (6). A comparison with Fig. 6b reveals their mirror symmetry about the plane $z = 1/2$. The case of $F_2 > F_1$ differs essentially from the case considered above: now, as seen from Figs. 6d and 6e, when the first (second) condition (6) is valid, the vortices of a larger (smaller) scale are generated. According to the stability analysis (we compare the location of points 5 and 6 in Fig. 4c), the second mode is unstable in the first of these cases, and from the first to the fourth modes are unstable with $|\gamma_3| > |\gamma_4| > |\gamma_2| \gg |\gamma_1|$ in the second case. Computations show that the $m = 4$ mode is actually realized. We point to qualitative agreement of Figs. 6a and 6b with Smeed's Figs. 17 and 18 [6], where the break of a three-layer vortex is pictured in a laboratory setup with similar parameters.

Cone-Shaped Vortex

The results of computations presented in this subsection show three variants to attain the mode of nonlinear instability with subsequent evolution of vortices at $h_1 = 0.1$, $h_2 = 0.2$, $h_3 = 0.7$; $F_1 = 1$, $F_2 = 4$; and $\Delta\alpha = 0.5$. The points in Fig. 5 numbered by Roman numerals correspond to the appropriate distributions of the potential vorticities, and the initial fields of the azimuth velocities in the layers are specified in Figs. 3f–3h.

Figure 7a exhibits the break in a vortex structure with tapering-down vortex patches, when the $m = 2$ mode is the most unstable. During the evolution, two pairs of vortices (hetons) [21] with inclined axes separate out from the peripheral part of the anticyclone in the top layer and the cyclone in the middle layer. These vortices move away from the center and rotate simulta-

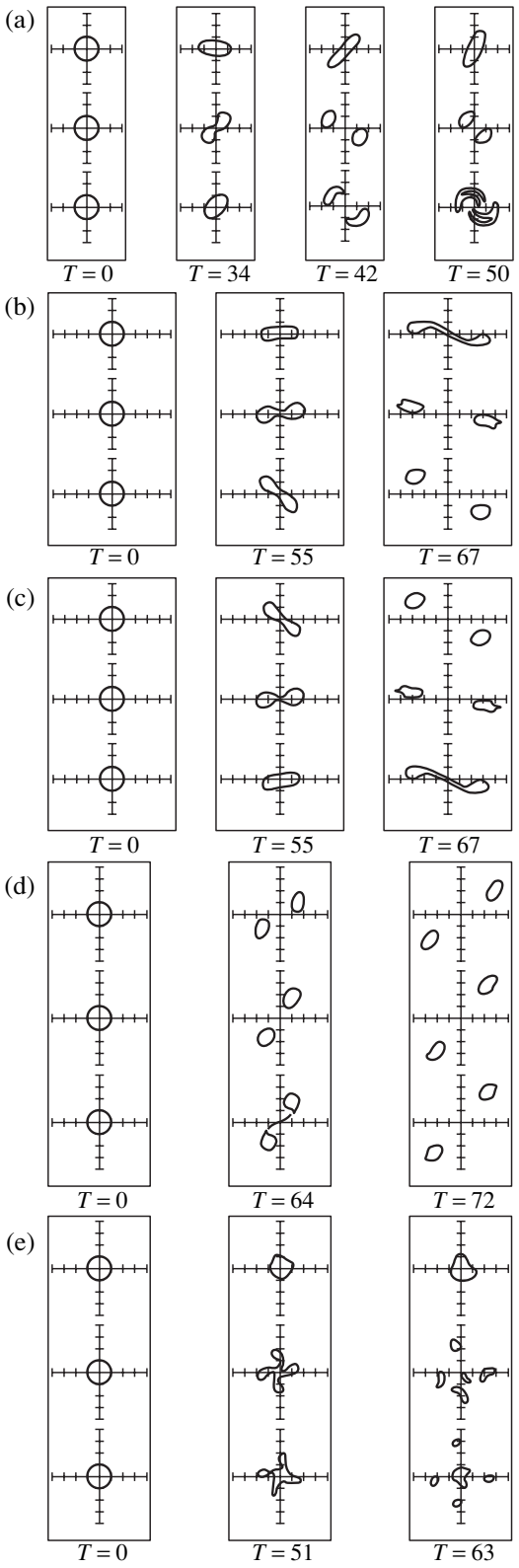

Fig. 6. Evolution of the unstable cylinder-shaped vortices under the conditions described by the points: (a) point 1 in Fig. 4a, (b) point 5 in Fig. 4a, (c) point 6 in Fig. 4a, (d) point 5 in Fig. 4c, (e) point *6* in Fig. 4c.

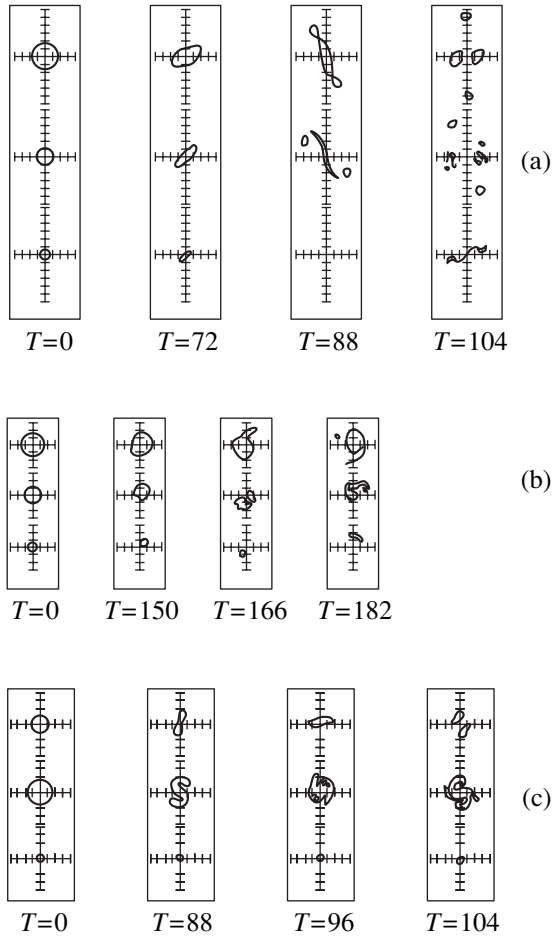

Fig. 7. The same as in Fig. 6, but for the cone-shaped vortices under the conditions described by the points: (a) point I in Fig. 5f, (b) point II in Fig. 5e, and (c) point III in Fig. 5f.

neously clockwise. The central part of the vortex spot in the middle layer is actually broken down, whereas that in the top layer is divided into two compact anticyclones rotating around the common center. Here, the contour of the patch in the bottom layer is a marker line.

An example of a vortex with the only first unstable mode is shown in Fig. 7b. Here, a helical motion of the entire vortex patch develops in time. It is accompanied by segregation of vortex filaments and fine vortices in the top layer and by division with subsequent merger and significant deformations of vortex contour in the middle layer. As the total intensity of the vortex is positive, it rotates counterclockwise. We note that, strictly speaking, the motion of the vortex as a whole does not fit the condition of immobility of its center of gravity. However, due to a multifold application of the contour surgery procedure, which allows for a mechanism of artificial dissipation, the conservation of all invariants cannot be guaranteed. For this reason, the vortex with an inclined axis not only rotates around its center but also begins to shift.

The evolution of a vortex that is barrel-shaped at the initial instant and has the minimum radius of the vortex patch in the bottom layer is shown in Fig. 7c. In this case, the most unstable mode in theory is the first one, whereas the numerical simulation demonstrates the realization of the $m = 2$ mode. The cyclonic vortex patch in the bottom layer virtually does not change its shape, while the cyclone in the middle layer undergoes deformations and "attempts" to keep its simple connectedness (at least, over the computational time). The top anticyclone alternatively splits up and merges forming a simply-connected figure, close to an ellipse. As a whole, we again observe a vortex structure similar to the above carousel but with vertical inversion.

CONCLUSION

We state the main results of the work. The stability of an isolated geostrophic three-layer vortex has been studied depending on its geometrical structure and fluid stratification. The numerical experiments on the break of unstable vortices have been performed with the aid of the three-layer method of contour dynamics model. The majority of them confirm the conclusions of the linear stability analysis. A baroclinic analogue of the tripole—carousel—has been obtained as a special case of the instability for the $m = 2$ mode. The versatility of tripoles must be emphasized. In a barotropic fluid, they can be formed as a result of the break of unstable axisymmetric vortices, unstable Karman's vortex streets [22–24], and a counter asymmetric collision of two dipoles [24, 25]. In a two-layer fluid, we observe a similar vortex structure as a result of a counter noncentral collision between two hetons with inclined axes [26, 27] and interaction of two initially close stationary hetons with vertical axes [28]. The instability of a three-layer vortex is stated above as a possible mechanism of its formation. The computations show that carousel-shaped structures are also observed for $m > 2$ (Fig. 6e).

It is shown that a more realistic description of vortex structure—the use of a conic shape rather than a cylindrical shape—promotes the conditions for forming unstable modes of lower orders. Theoretically, the $m = 1$ mode is the most unstable for cone-shaped vortices. However, the computations point to the tendency for realization of the second mode.

We note that the necessary condition of instability, which is, as seen from Figs. 4 and 5, the requirement that the vertical distribution of the potential vorticity must change its sign along the vertical at least once, appears to be not unduly rigid for ocean vortices. For example, the tendency of ocean currents to compensate locally for water discharge has been indicated in [29] (this condition is fulfilled in our experiments illustrated by Figs. 6b–6e). The kinematic vertical structure of the vortex observed in the Northwestern Pacific (the Megapoligon experiment, June–November, 1987) has been briefly described in [29]. The vortex had a greater size

at a depth of 1200 m than in the upper layers, and its velocities were significant. The evolution of a vortex with similar structure is shown in Fig. 7c.

It is believed that the stability investigation of variously shaped vortices of form (5) can be useful in understanding mechanisms of the break of ocean vortices.

ACKNOWLEDGMENTS

This work was carried out at the Pacific Oceanological Institute, Far East Division, Russian Academy of Sciences. The author is grateful to V.F. Kozlov for encouragement and useful discussions, V.G. Makarov for help in using the program codes [15, 16], V.M. Gryanik, E.M. Dobryshman, F.V. Dolzhanskii, V.N. Zyryanov, M.V. Kurganskii for their participation in discussions of the results, and O.I. Yakovenko for organizing the figures.

APPENDIX

Omitting simple but cumbersome calculations, we write down the relations for $T_{in}^{(j)}$ and U_j from (15) for the first of variants (5) when $\alpha_1 \geq \alpha_2 \geq \alpha_3$:

$$T_{12}^{(0)} = \frac{1}{2}\left(\frac{\alpha_2}{\alpha_1}\right)^{m-1}, \quad T_{13}^{(0)} = \frac{1}{2}\left(\frac{\alpha_3}{\alpha_2}\right)^{m-1},$$

$$T_{21}^{(0)} = \frac{1}{2}\left(\frac{\alpha_2}{\alpha_1}\right)^{m+1},$$

$$T_{23}^{(0)} = \frac{1}{2}\left(\frac{\alpha_3}{\alpha_2}\right)^{m-1}, \quad T_{31}^{(0)} = \frac{1}{2}\left(\frac{\alpha_3}{\alpha_1}\right)^{m+1},$$

$$T_{32}^{(0)} = \frac{1}{2}\left(\frac{\alpha_3}{\alpha_2}\right)^{m+1},$$

$$T_{12}^{(j)} = \frac{\alpha_1}{\alpha_2} m I_m(k_j\alpha_2) K_m(k_j\alpha_1),$$

$$T_{13}^{(j)} = \frac{\alpha_1}{\alpha_3} m I_m(k_j\alpha_3) K_m(k_j\alpha_1),$$

$$T_{21}^{(j)} = \frac{\alpha_2}{\alpha_1} m I_m(k_j\alpha_2) K_m(k_j\alpha_1),$$

$$T_{23}^{(j)} = \frac{\alpha_2}{\alpha_3} m I_m(k_j\alpha_3) K_m(k_j\alpha_2),$$

$$T_{31}^{(j)} = \frac{\alpha_3}{\alpha_1} m I_m(k_j\alpha_3) K_m(k_j\alpha_1),$$

$$T_{32}^{(j)} = \frac{\alpha_3}{\alpha_2} m I_m(k_j\alpha_3) K_m(k_j\alpha_2),$$

$$U_0(\alpha_1) = \frac{1}{2}(s_{11}\Pi_1\alpha_1^2 + s_{12}\Pi_2\alpha_2^2 + s_{13}\Pi_3\alpha_3^2)/\alpha_1,$$

$$U_0(\alpha_2) = \frac{1}{2}((s_{11}\Pi_1 + s_{12}\Pi_2)\alpha_2 + s_{13}\Pi_3\alpha_3^2/\alpha_2),$$

$$U_0(\alpha_3) = \frac{1}{2}(s_{11}\Pi_1 + s_{12}\Pi_2 + s_{13}\Pi_3)\alpha_3,$$

$$U_j(\alpha_1) = K_1(k_j\alpha_1)(s_{j+1,1}\Pi_1\alpha_1 I_1(k_j\alpha_1) + s_{j+1,2}\Pi_2\alpha_2 I_1(k_j\alpha_2) + s_{j+1,3}\Pi_3\alpha_3 I_1(k_j\alpha_3)),$$

$$U_j(\alpha_2) = s_{j+1,1}\Pi_1 I_1(k_j\alpha_2)(2\alpha_2 K_1(k_j\alpha_2) - \alpha_1 K_1(k_j\alpha_1)) + s_{j+1,2}\Pi_2\alpha_2 I_1(k_j\alpha_2) K_1(k_j\alpha_2) + s_{j+1,3}\Pi_3\alpha_3 I_1(k_j\alpha_3) K_1(k_j\alpha_2),$$

$$U_j(\alpha_3) = I_1(k_j\alpha_3)(s_{j+1,1}\Pi_1(2\alpha_3 K_1(k_j\alpha_3) - \alpha_1 K_1(k_j\alpha_1)) + s_{j+1,2}\Pi_2(2\alpha_3 K_1(k_j\alpha_3) - \alpha_2 K_1(k_j\alpha_2)) + s_{j+1,3}\Pi_3\alpha_3 K_1(k_j\alpha_3)).$$

Here $j = 1, 2$; $m \leq 1$. The structure of these formulas for the other five variants (5) is similar.

REFERENCES

1. Holmboe, J., Instability of Baroclinic Three-Layered Models of the Atmosphere, *Geophys. Publ.*, 1968, vol. 28, pp. 1–27.
2. Davey, M.K., Baroclinic Instability of a Fluid with Three Layers, *J. Atmos. Sci*., 1977, vol. 34, pp. 1224–1234.
3. Wright, D.G., On the Stability of a Fluid with Specialized Density Stratification. Part I: Baroclinic Instability and Constant Bottom Slope, *J. Phys. Oceanogr.*, 1980, vol. 10, pp. 639–666.
4. Ikeda, M., Linear Instability of a Current Flowing along a Bottom Slope Using a Three-Layer Model, *J. Phys. Oceanogr.*, 1993, vol. 13, pp. 208–223.
5. Smeed, D.A., Baroclinic Instability of Three-Layer Flows. Part 1. Linear Stability, *J. Fluid Mech*., 1988, vol. 194, pp. 217–231.
6. Smeed, D.A., Baroclinic Instability of Three-Layer Flows. Part 2. Experiments with Eddies, *J. Fluid Mech.*, 1988, vol. 194, pp. 233–259.
7. Mirabel', A.P. and Monin, A.S., On the Instability of Ocean Gyres, *Dokl. Akad. Nauk SSSR*, 1988, vol. 303, pp. 976–979.
8. Mirabel', A.P. and Monin, A.S., On the Instability of a Gyre in a Continuously Stratified Ocean, *Dokl. Akad. Nauk SSSR*, 1988, vol. 309, pp. 716–720.
9. Mirabel', A.P. and Monin, A.S., On the instability of Sverdrup's Gyre in Three-Layer and Continuously Stratified Oceans, *Izv. Akad. Nauk SSSR, Fiz. Atmos. Okeana*, 1990, vol. 26, pp. 63–71.
10. Sokolovskiy, M.A., Modeling of Three-Layer Vortex Motions in the Ocean by the Contour Dynamics Method, *Izv. Akad. Nauk SSSR, Fiz. Atmos. Okeana*, 1991, vol. 27, no. 5, pp. 550–562.

11. Polvani, L.M., Zabusky, N.J., and Flierl, G.R., Two-Layer Geostrophic Vortex Dynamics. Part 1. Upper-Layer V-States and Merger, *J. Fluid Mech*., 1989, vol. 205, pp. 215–242.
12. Kamenkovich, V.M., Koshlyakov, M.N., and Monin, A.S., *Sinopticheskie vikhri v okeane* (Synoptic Eddies in the Ocean), Leningrad: Gidrometeoizdat, 1987.
13. Flierl, G.R., On the Instability of Geostrophic Vortices, *J. Fluid Mech*., 1988, vol. 197, pp. 339–344.
14. Hairer, E., Nörsett, S., and Wanner, G., *Solving Ordinary Differential Equations. Nonstiff Problems*, Berlin: Springer, 1987. Translated under the title *Reshenie obyknovennykh differentsial'nykh uravnenii. Nezhestkie zadachi*, Moscow: Mir, 1990.
15. Makarov, V.G., A Program Code for Investigation of Plane Vortex Currents in an Ideal Fluid by the Method of Contour Dynamics, *Metod konturnoi dinamiki v okeanologicheskikh issledovaniyakh* (The Method of Contour Dynamics in Oceanological Investigations), Vladivostok: Far East Division, USSR Acad. Sci.,1990, pp. 28–39.
16. Makarov, V.G., A Computational Algorithm of the Method of Contour Dynamics with Changeable Topology of the Domains under Study, *Model. Mekh*., 1991, vol. 5(22), no. 4, pp. 83–95.
17. Leith, C.E., Minimum Enstrophy Vortices, *Phys. Fluids*., 1984, vol. 27, pp. 1388–1395.
18. Polvani, L.M., Two-Layer Geostrophic Vortex Dynamics. Pt. 2. Alignment and Two-Layer V-States, *J. Fluid Mech*., 1991, vol. 225, pp. 241–270.
19. Gryanik, V.M. and Tevs, M.V., Dynamics of Singular Geostrophic Vortices in the *N*-Layer Model of the Atmosphere (Ocean), *Izv. Akad. Nauk SSSR, Fiz. Atmos. Okeana*, 1989, vol. 25, no. 3, pp. 243–256.
20. Verron, J., Hopfinger, E.J., and McWilliams, J.C., Sensitivity to Initial Conditions in the Merging of Two-Layer Baroclinic Vortices, *Phys. Fluids A*, 1990, vol. 2, pp. 886–889.
21. Hogg, N.G. and Stommel, H.M., The Heton, an Elementary Interaction between Discrete Baroclinic Geostrophic Vortices, and Its Implication Concerning Eddy Heat-Flow, *Proc.R. Soc. A*, 1985, vol. 397, pp. 1–20.
22. Polvani, L.M. and Carton, X.J., The Tripole: A New Vortex Structure of Incompressible Two-Dimensional Flow, *Geophys. Astrophys. Fluid. Dyn*., 1990, vol. 51, pp. 87–102.
23. Carton, X.J., Flierl, G.R., and Polvani, L.M., The Generation of Tripoles from Unstable Axisymmetric Isolated Vortex Structures, *Europhys. Lett.*, 1989, vol. 9, pp. 339–344.
24. Orlandi, P. and van Heijst, G.J.F., Numerical Simulation of Tripolar Vortices in 2D Flow, *Fluid Dyn. Res*., 1992, vol. 9, pp. 179–206.
25. Larichev, V.D. and Reznik, G.M., On the Collision of Two-Dimensional Solitary Rossby Waves, *Okeanologiya*, 1983, vol. 23, no. 5, pp. 725–734.
26. Sokolovskiy, M.A., On the Counter Collision of Distributed Hetons, *Dokl. Akad. Nauk SSSR*, 1989, vol. 306, pp. 198–202.
27. Sokolovskiy, M.A., Numerical Simulation of the Interaction of Distributed Hetons in a Counter Collision, *Metod konturnoi dinamiki v okeanologicheskikh issledovaniyakh* (The Contour Dynamics Method in Oceanological Investigations), Vladivostok: Far East Division, USSR Acad. Sci., 1990, pp. 40–57.
28. Sokolovskiy, M.A., Interaction of Distributed Hetons, *Preprint of Pacific Oceanological Inst., Far East Division, USSR Acad. Sci.*, Vladivostok, 1990.
29. Monin, A.S. and Zhikharev, G.M., Ocean Eddies, *Usp. Fiz. Nauk*, 1990, vol. 160, no. 5, pp. 1–47.